Porous silica nanosheets in PIM-1 membranes for CO_2 separation

Sajjad Mohsenpour [a], Zunmin Guo [a,**], Faiz Almansour [a], Stuart M. Holmes [a], Peter M. Budd [b], Patricia Gorgojo [a,c,d,*]

[a] *Department of Chemical Engineering, Faculty of Science and Engineering, The University of Manchester, Manchester, M13 9PL, United Kingdom*
[b] *Department of Chemistry, Faculty of Science and Engineering, The University of Manchester, Manchester, M13 9PL, United Kingdom*
[c] *Instituto de Nanociencia y Materiales de Aragón (INMA) CSIC-Universidad de Zaragoza, C/ Mariano Esquillor s/n, 50018, Zaragoza, Spain*
[d] *Departmento de Ingeniería Química y Tecnologías del Medio Ambiente, Universidad de Zaragoza, C/ Pedro Cerbuna 12, 50009, Zaragoza, Spain*

ARTICLE INFO

ABSTRACT

PIM-1-based freestanding mixed matrix membranes (MMMs) and thin film nanocomposites (TFNs) were prepared by incorporating porous silica nanosheets (SN) and exfoliated SN (E-SN) derived from natural vermiculite (Verm) in the PIM-1 polymer matrix. In addition, SN were functionalized by sulfonic acid and amine groups (S-SN and N-SN, respectively) and were also used as fillers for the preparation of MMMs. The gas separation performance was evaluated using CO_2/CH_4 and CO_2/N_2 (1:1, v:v) binary gas mixtures. Among freestanding membranes, fresh ones (i.e. tested right after preparation) containing 0.05 wt% functionalized SN and E-SN outperformed the neat PIM-1, surpassing the 2008 Robeson upper bound. At the same filler concentration, fresh MMMs with sulfonic acid-functionalized SN (S-SN) exhibited 40% higher CO_2 permeability, 20% higher CO_2/N_2 selectivity and almost the same CO_2/CH_4 selectivity as neat PIM-1 membranes. Moreover, after 150 days of aging, these membranes were capable of maintaining up to 68% of their initial CO_2 permeability (compared to 37% for neat PIM-1). When prepared as TFN membranes, the incorporation of 0.05 wt% of S-SN led to 35% higher initial CO_2 permeance and five times higher CO_2 permeance after 28 days.

1. Introduction

Membrane technology for CO_2 separation is a growing field that has demonstrated its feasibility in the gas sweetening industry [1], and is currently widely investigated for the upgrading of biogas [2], and the capture of CO_2 from flue gases in the power industry. However, advanced membrane materials with tailored structures are needed to expand their use and for the design of more competitive processes.

High free volume polymer of intrinsic microporosity PIM-1 shows a combination of high CO_2 permeability and good CO_2/CH_4 and CO_2/N_2 selectivity [3]. Its outstanding performance contributed to revisiting the Robeson upper bound in 2008 [4]. However, the very high free volume in this superglassy polymer, and thus its high initial gas permeability, are lost over time. This phenomenon is known as physical aging and takes place due to the rearrangement of polymer chains toward an unattainable equilibrium state [5]. This effect is even more pronounced for thin film composite (TFC) membranes [6], which is the preferred

configuration for commercial gas separation applications (flux is inversely proportional to membrane thickness). It has been reported that flux declines from 2400 GPU to 600 GPU in just 28 days for PIM-1 thin films [7]. Therefore, advances on physical aging inhibition for PIM-1 are needed to make it feasible in large scale applications.

Different strategies have been proposed to prevent aging, such as rigidification of polymer structure by changes to the polymer backbone [5] and by cross-linking of polymer chains [8], mostly in thick freestanding PIM-1 films. However, these methods can reduce the initial permeability [9]. On the other hand, the fabrication of PIM-1-based mixed matrix membranes (MMMs) by blending with porous [7,10] and nonporous fillers [2,11,12] has shown promising results.

Embedding nonporous materials in polymers usually increases the tortuosity and gas barrier properties of gas molecules [13], while the addition of porous fillers can enhance gas transport. However, the incorporation of porous and nonporous nanoparticles (NPs) can also alter the polymer chain packing, increasing the free volume and thus gas

---

* Corresponding author. Departmento de Ingeniería Química y Tecnologías del Medio Ambiente, Universidad de Zaragoza, C/ Pedro Cerbuna 12, 50009 Zaragoza, Spain.
** Corresponding author.
E-mail addresses: zunmin.guo@manchester.ac.uk (Z. Guo), pgorgojo@unizar.es (P. Gorgojo).

permeability. In addition, they can lead to the formation of interfacial voids between the filler and polymer chains, which is also accompanied by an increase in gas permeability and a decrease in selectivity [14]. Sakaguchi et al. [15] studied the CO_2/N_2 separation performance of PIM-1-based MMMs containing amine, methyl and carboxylic-functionalized nonporous silica NPs. The incorporation of amine and carboxylic-functionalized silica led to membranes with higher CO_2 permeability and lower selectivity, and membranes with methyl-modified silica exhibited both higher permeability and selectivity than neat PIM-1. The latter also revealed better long-term stability compared to neat PIM-1 with almost constant permeability over 60 days for the freestanding membranes. Kinoshita et al. [7] also reported an enhancement in the anti-aging performance of PIM-1 MMMs fabricated from amine and nitro-functionalized polyhedral oligomeric silsesquioxane (POSS) (silica-based) nanofillers for both freestanding and supported thin films (known as thin film nanocomposite membranes, TFNs). Yet, the CO_2 permeance dropped by ~90% for the TFNs over a month.

In this investigation, highly porous few-layer silica nanosheets (SN) and exfoliated SN were synthesized and used as fillers in freestanding and TFN PIM-1 membranes for the first time. SN can be easily synthesized via a simple and environmentally benign acid-treatment method from Vermiculite (Verm), which is a cheap aluminosilicate mineral with a layered structure containing crystalline aluminium octahedral sheets and exchangeable cations (such as Mg^{2+}, Ca^{2+}, Na^+ and K^+) sandwiched between two tetrahedral sheets of silica (Fig. 1) [16]. Due to its low price, layered structures and excellent ion-exchange properties, Verm has been explored as membrane filler [16], adsorbent [17], nanofluidic channel network [18], and electrode material [19]. To the best of our knowledge, the gas separation applications using Verm or its derivations have not been reported until now.

It has been reported that fillers with polar functional groups (i.e. amine [20] and sulfonic [21]) can interact with the quadrupole moment of CO_2 molecules and result in an increase in the CO_2 solubility of the MMMs. Herein, sulfonic acid functionalized SN and amine functionalized SN were used separately as a filler to increase the compatibility of

the filler with the polymer matrix and study the possible interaction between CO_2 and the membranes. The fabricated membranes in this study were tested for CO_2/CH_4 and CO_2/N_2 separation for up to 150 days (freestanding membranes) and up to 28 days (TFN membranes) to evaluate aging behaviour.

2. Experimental

2.1. Materials

For PIM-1 synthesis, monomers of 3,3,3′,3′-tetramethyl-1,1′-spirobisindane-5,5′,6′,6′-tetrol, 97% (TTSBI) and 2,3,5,6-tetrafluoroterephthalonitrile, 98% (TFTPN) were purchased from Alfa Aesar (UK) and Fluorochem Limited (UK), respectively. TTSBI was purified as previously reported by Ameen et al. [12]. Anhydrous potassium carbonate (K_2CO_3) was purchased from Fisher Scientific UK Ltd. Chloroform and methanol (MeOH) were purchased from Fisher Chemical. N,N-dimethylacetamide (DMAc), 1,2-dichlorobenzene (DCB), and isopropyl alcohol (IPA) were supplied by Sigma Aldrich (UK). Polyacrylonitrile (PAN) membrane supports were kindly supplied by Saudi Arabian Oil Company and used for the preparation of thin film composite and nanocomposite membranes.

For the synthesis of SN and functionalized SN, Verm, (3-mercaptopropyl)trimethoxysilane (MPTMS), (3-aminopropyl)triethoxysilane (APTES), aqueous hydrochloric acid (HCl, 34 wt%), dichloromethane (DCM) and toluene were purchased from Sigma-Aldrich (UK). Hydrogen peroxide (H_2O_2, 30%) was acquired from VWR Chemicals (UK). Ethanol was purchased from Fisher Chemical. Deionized (DI) water was produced in-house by a Milli-Q integral system (Merck Millipore, Ireland).

2.2. PIM-1 synthesis

PIM-1 was synthesized according to the procedure reported by Tammaddondar et al. [22]. An equimolar ratio of the monomers, TTBSI (10.212 g, 0.03 mol) and TFTPN (6.003 g, 0.03 mol), and K_2CO_3 (12.483 g, 0.09 mol) as a base, were added to a 250 mL three neck round bottom flux with a Dean-Stark trap to remove water as a by-product from the reaction mixture. The mixture was stirred at room temperature for 30 min under continuous nitrogen flow. Then, 60 mL DMAc and 30 mL DCB were added to the mixture, and the temperature was increased to 160 °C. The reaction time was ~36 min including the time required to increase the temperature from room temperature to 160 °C (~16 min). At the end of the reaction, the hot yellow viscous solution was poured into 200 mL MeOH, precipitating as a thread-like PIM-1 polymer. After 6 h, the precipitate was filtered and dried and dissolved in chloroform overnight. The solution was again precipitated by MeOH and then washed using DI water under reflux at 95 °C for 16 h. The PIM-1 powder was dried and washed with 50 mL 1,4 dioxane, 200 mL acetone and 200 mL MeOH, respectively. The final product was dried at 120 °C for 48 h.

2.3. Silica nanosheets (SN) synthesis

Natural Verm with the chemical formula $(Al_{0.30}Ti_{0.04}Fe_{0.63}Mg_{2.00})(Si_{3.21}Al_{0.79})O_{10}(OH)_2 Mg_{0.13}Na_{0.02} K_{0.10}(H_2O)_n$ [23] (Fig. 1) was used as a precursor to prepare SN by the acid-leaching method [16]. Briefly, 3 g of Verm and 100 mL 2 M HCl were mixed at 50 °C for 8 h under stirring. The decanted solution was washed with DI water until the filtrate had a pH of 7. The obtained powder was dried in vacuum oven overnight at 70 °C and then was finally ground in an agate mortar for 20 min.

2.3.1. Synthesis of exfoliated few-layer SN

In order to obtain exfoliated few-layer SN (E-SN), the liquid phase exfoliation (LPE) method [16] was followed; ground SN was dispersed in ethanol (1 mg mL^{-1}) for 2 h by a Hielscher Ultrasonic Processor
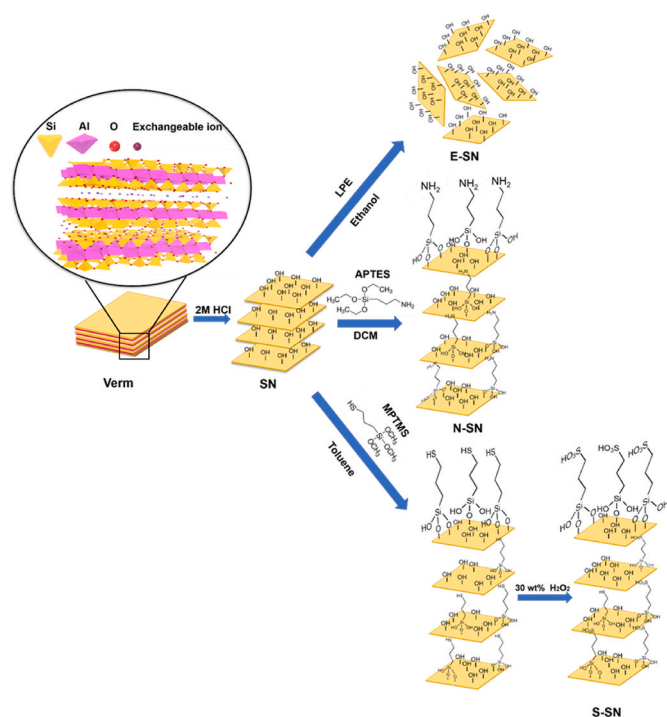

Fig. 1. Schematic of SN, E-SN, N-SN and S-SN preparation (modified from Ref. [16]).

(UP200St) instrument, and the solution was subsequently centrifuged at 1000 rpm for 10 min to remove non-exfoliated SN and big particles. The supernatant was then decanted and the final product was dried in a vacuum oven. A schematic of SN and E-SN preparation is shown in Fig. 1.

2.3.2. Amine functionalization of SN

Amine-functionalized SN (N-SN) was prepared by dispersing 0.1 g of SN in a well-mixed solution containing 0.1 mL APTES and 3 mL DCM as reported elsewhere [27]. The solution was stirred for 24 h at room temperature, centrifuged at 8000 rpm for 15 min, filtered, washed with ethanol and DI water several times, and dried at 40 °C overnight under vacuum. The procedure is summarized in Fig. 1.

2.3.3. Sulfonic acid functionalization of SN

The sulfonated SN (S-SN) was carried out through silane condensation [24]. Ground SN, MPTMS and toluene with a weight ratio of 1:2:20, were mixed at 110 °C for 24 h. The final solution was centrifuged at 10000 rpm for 12 min and the precipitate was washed with ethanol and DI water several times. The obtained powder was thiol (-SH) grafted SN. To convert thiol groups to sulfonic groups, the dried powder was mixed with H_2O_2 solution for 24 h and washed with ethanol and DI water. The final product was dried at 40 °C overnight. The synthesis procedure of S-SN is shown in Fig. 1.

2.4. Membrane Fabrication

2.4.1. Thick freestanding membrane preparation

Thick freestanding membranes (thickness ~ 50–80 μm) containing 0.05, 0.1, 0.25 and 1 wt% of fillers (SN, E-SN and functionalized SN) were prepared by the solvent evaporation method in petri dishes. The required amount of silica nanosheets or derivatives for each membrane (calculated relative to the PIM-1 in the final membrane) was first mixed with 10 mg of PIM-1 powder and dissolved in chloroform (1.6 ml) via magnetic stirring for 2 h (process known as priming that is carried out to minimize filler agglomeration). Subsequently, the remaining PIM-1 powder (40 mg) was added to the solution and was stirred for 6 h at room temperature followed by sonication in a sonication bath (80 kHz frequency at 100% power). The solution was cast in a 3 cm glass petri dish and covered with a lid to slow down the rate of chloroform evaporation. After 24 h, the solidified film was soaked in MeOH for 8 h to increase the fractional free volume of the membrane and remove solvent residue from the membrane [25]. Finally, the membranes were dried for 8 h at 80 °C under vacuum. For each filler concentration, 3 to 4 membrane discs were prepared and tested for gas separation. Membrane thickness measurements were carried out using a digital micrometer (Mitutoyo Corporation) with an accuracy of ±0.5 μm at 5 different points of the membrane and the average values and standard deviations are reported in Table S.3.

2.4.2. Thin-film membrane preparation

Thin film composite and nanocomposite membranes (TFC and TFN, respectively) were prepared by coating porous PAN supports using an in-house built roll-coating system, as reported elsewhere [26] and shown in Fig. 2. The PIM-1 concentration employed in all coating solutions was 2 wt% in chloroform (10 mL). For the TFN membranes filler loadings of 0.05 wt% relative to PIM-1 were added. Additional membranes at a concentration of 0.25 wt% of S-SN were prepared. All membranes were dried in a vacuum oven at 25 °C overnight and 10 mbar prior to testing.

2.5. Characterization of materials and membranes

The average molar mass of PIM-1 polymer was obtained using gel permeation chromatography (GPC, Viscotek GCPmax VE 2001 chromatograph (Malvern, UK)), as detailed in a previous publication [27]. Proton nuclear magnetic resonance (^{1}H NMR) was carried out using a
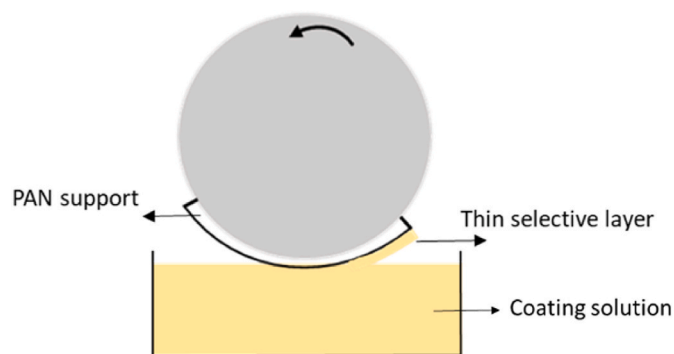

Fig. 2. Schematic of the fabrication of thin film membranes via a roll-coating technique.

Bruker DPX 400 MHz spectrometer to confirm the structure of the PIM-1 polymer. To further study the topology of the synthesized PIM-1 in the low range of molar mass (<10000 g mol^{-1}), matrix-assisted laser desorption/ionization-time of flight (MALDI-TOF) mass spectrometry was carried out on a Shimadzu Biotech Axima Confidence instrument. Brunauer-Emmett-Teller (BET) surface area of synthesized PIM-1 was calculated from the nitrogen (N_2) adsorption isotherm acquired by a Micromeritics ASAP 2020. Following the same procedure, BET surface area, pore volume (V_p) and pore diameter (d_p) were calculated for the fillers.

Fourier transform infrared (FTIR) spectroscopy (Tensor 27 FTIR spectrometer) and X-ray photoelectron spectroscopy (XPS, Kratos Axis SUPRA) were carried out to study the chemical structures of Verm, and the fillers. In addition, potential interactions between the fillers and the polymer chains were investigated by FTIR. Thermogravimetric analysis (TGA, TGA550 thermal analyzer) was employed to study the thermal stability of the precursor Verm, the fillers and the membranes, heating from 40 to 800 °C at a rate of 10 °C min^{-1} under nitrogen gas. The crystallinity of the inorganic materials and prepared membranes were studied using X-Ray diffraction (XRD) in 2θ range of 2.5–30° for the SNs and 4–40° for the membranes. The d-spacing of the fillers was calculated according to Bragg's law (equation (1)) [28].

$$d = \frac{\lambda}{2 \sin \theta} \tag{1}$$

where, λ (0.154 nm) is the wavelength of the X-ray beam and θ (in degree) is the diffraction angle.

The average lateral flake size of the fillers was measured using a scanning electron microscope (SEM, FEI Quanta 250 FEG-SEM). Prior to SEM imaging of the fillers, dilute solutions (10 ppm) in chloroform were prepared and drop coated on a clean silicon dioxide wafer. The cross-section and surface morphology of the membranes were also studied by SEM. Membrane samples were prepared by snap freezing in liquid nitrogen, fracturing and coating with a thin layer of platinum. Energy dispersive X-ray spectroscopy (EDS) maps were collected using the AZtec 3.3 SP1 software to study the presence and distribution of fillers in the polymer matrices.

2.6. Gas separation performance

2.6.1. Thick freestanding membranes

The gas separation performance of thick membranes was evaluated for binary mixtures of CO_2/CH_4 (1:1, v:v) or CO_2/N_2 (1:1, v:v) in a constant pressure (~2 bar) variable volume method system, as reported in more detail elsewhere [12]. The permeate side was kept at atmospheric pressure and the membrane cell and feed gas at 25 °C throughout the testing. The permeate gas was analysed using an Agilent 490 microGC gas chromatograph and helium gas was used to sweep the permeate gas to the microGC. Fresh membranes were tested one day

after preparation and their gas permeabilities (P_i) in Barrer (1 Barrer = 10^{-10} cm^3(STP).cm cm^{-2}. s^{-1}.cmHg^{-1}) were determined according to equation (2):

$$P_i = \frac{Q_i L}{A(y_i p_f - x_i p_p)} \times 10^{10} \qquad (2)$$

where Q_i (cm^3 (STP) s^{-1}) is the gas flow rate on the permeate side, p_f (cmHg) and p_p (cmHg) are the feed and permeate side pressures, respectively. y_i and x_i are the fraction of gas in the feed and permeate sides, respectively. L (cm) is the membrane thickness, and A (cm^2) is the effective membrane area.

In order to preserve the integrity of the membranes and be able to retest for gas separation after several weeks/months, membrane discs were sandwiched between two circular pieces of aluminium with concentric circular holes and sealed with epoxy resin. The effective membranes areas available for gas permeation after the sealing were calculated by ImageJ software and were ~0.1 cm^2.

The selectivity of the membranes was calculated as the ratio of permeabilities (faster over slower permeating gases) according to equation (3).

$$\alpha_{A/B} = \frac{P_A}{P_B} \qquad (3)$$

To evaluate effects of physical aging on the gas permeability, the membranes were kept in sealed petri dishes and retested for CO$_2$/CH$_4$ separation after 45, 110 and 150 days. The relative CO$_2$ permeability and the CO$_2$ permeability drop over time were calculated according to equations (4) and (5), respectively.

$$\text{Relative } P_{CO_2} = \frac{P_{CO_2}^{\text{aged at } t_1}}{P_{CO_2}^{\text{fresh}}} \qquad (4)$$

$$\text{Permeability drop} = P_{CO_2}^{\text{fresh}} - P_{CO_2}^{\text{aged at } t_1} \qquad (5)$$

where t_1 (days) is the aging time of the membrane.

To gain a better understanding of the role of the fillers in the MMMs, the solubility (S) and diffusion (D) coefficients of the membranes were determined. In this regard, single gas (CO$_2$ and CH$_4$) permeation experiments of 180 days aged membranes were carried out using a time-lag instrument at room temperature (18–22 °C). Details of the time-lag instrument that was used are reported elsewhere [12]. The measurements were carried out using the constant-volume variable pressure method at a feed side pressure of 1.2 bar. Prior to the gas separation measurements, both feed and permeate sides were vacuumed for at least 3 h using an Edwards T-Station Turbo Pumping Station 75 equipped with an EXT75DX turbopump and an E2M1.5 rotary vane oil-sealed pump. The initial permeate side pressure was 10^{-3} mbar and after introducing the feed, pressure increase was recorded via a MKS baratron gauge with an accuracy of 10^{-4} mbar for 500 s at time intervals of 1 s. The pure gas permeability (P_i, Barrer) was calculated according to equations (6) and (7):

$$O_i = \frac{V_P \vartheta_{STP}}{RT} \times \frac{dp}{dt} \qquad (6)$$

$$P_i = \frac{O_i L}{A \Delta p} \times 10^{10} \qquad (7)$$

where, V_P (53.68 cm^3) is the permeate cell volume, ϑ_{STP} (22400 cm^3 mol^{-1}) is the molar volume of the gas at STP. R (6236 cmHg.cm^3 K^{-1}. mol^{-1}) is gas constant and T (K) is the absolute temperature. Δp (cmHg) is the average transmembrane pressure difference. L (cm) and A (cm^2) are the membrane thickness and membrane effective area, respectively. $\frac{dp}{dt}$ (cmHg s^{-1}) is the build-up of permeate side pressure. The diffusion and solubility coefficients were calculated using the following equations [29]:

$$D_i = \frac{L^2}{6\tau_i} \qquad (8)$$

$$S_i = \frac{P_i}{D_i} \qquad (9)$$

where τ (s) is the time-lag.

2.6.2. Thin film supported membranes

Single gas permeation tests of the prepared thin film supported membranes were carried out in the setup shown in Fig. S.1 of the supporting information. Measurements were performed using CO$_2$ and CH$_4$ at room temperature (18–22 °C). The feed side pressure was kept around 2 bar while the permeate side was at atmospheric pressure. The volumetric flow rate of the permeate gas was determined using a bubble flowmeter and the gas permeance was calculated according to equation (10):

$$K = \frac{Q}{A \Delta p} \times 10^6 \qquad (10)$$

where K is gas permeance in gas permeation unit (GPU, 1 GPU = 10^{-6} cm^3[STP] cm^{-2}.s^{-1}.cmHg^{-1}), Q (cm^3 (STP) s^{-1}) is the volumetric flow rate of permeate gas and Δp is the transmembrane pressure difference. The effective membrane area (A) was 2.1 cm^2. The permeance values of thin membranes were converted to permeability using equation (11):

$$P = K \times l \times 10^4 \qquad (11)$$

where l (cm) is the selective layer thickness and was calculated using cross-sectional SEM images of the membranes. TFC and TFN membranes were retested after 7 and 28 days to evaluate physical aging. At least two membranes were tested for each concentration and filler, and the average results along with the standard deviation are reported. It should be noted that individual coupons of TFC and TFN membranes were tested only once, as enough coupons could be obtained from the prepared membranes (PIM-1-coated supports of rectangular shape with dimensions 2.5 × 6 cm) for the testing of fresh and aged samples. This way potential damage due to the repeated gas separation tests can be avoided [30].

3. Results

3.1. Materials characterization

3.1.1. PIM-1 characterization

The synthesized PIM-1 has a weight-average molar mass (M_w) of 88.8 kg mol^{-1} and a number-average molar mass (M_n) of 45.4 kg mol^{-1}. The double logarithmic plot of the Mark-Houwink equation (shown in Fig. S.2) shows a reduction in the slope towards higher molar mass, which could be explained by the presence of more compact structures such as branched and cyclic polymer chains (Fig. S.3) [31]. The main peaks in the low molecular weight fraction of the MALDI-TOF spectrum (Fig. S.4) are assigned to cyclic PIM-1 structures. Small fragmentation product peaks, which may originate from the branched structures [12, 31], are also observed. The presence of some branched structures in the PIM-1 is confirmed by the ^{1}H NMR spectrum (Fig. S.5). The BET surface area of the synthesized PIM-1 is 721.9 ± 7.4 m^2 g^{-1} (N$_2$ adsorption-desorption isotherms shown in Fig. S.6a), in the range of reported data in literature (630–899 m^2 g^{-1}) [30].

3.1.2. Filler characterization

The BET surface area, pore volume (V_p (cm^3 g^{-1})) and pore size (D_p (nm)) of the various silica nanosheets used as fillers for the preparation of membranes are shown in Table S.2 of the supporting information. The surface area of SN (449 m^2 g^{-1}) is 64 times higher than that of the layered precursor Verm (7 m^2 g^{-1}), and also the pore volume increased

from 0.02 cm^3 g^{-1} for Verm to 0.37 cm^3 g^{-1} for SN. This increase in porosity and the formation of larger cavities (typically mesopores) confirms the removal of exchangeable cations by the acid-leaching process [16]. The N$_2$ adsorption-desorption isotherms of the SN and Verm are shown in Fig. S.6. Upon functionalization of SN there is a reduction in their BET areas; 251 and 318 m^2 g^{-1} for N-SN and S-SN, respectively. This may be ascribed to pore blocking by the long alkyl chains of the functional groups, as reported by Abdelsamat et al. in the functionalization of mesoporous silica NPs [32]. The mesoporous structure of the SN seems to be unaltered upon functionalization as confirmed by the relatively similar adsorption-desorption isotherms for all SN samples (Fig. S.6c&d in the supporting information). The exfoliated sample prepared via sonication of SN, E-SN, shows a BET area of 364 m^2 g^{-1}. This lower value as compared to SN may be due to partial agglomeration and restacking of the exfoliated layers, as confirmed by the presence of large particles in the SEM images in Fig. S.7. SEM images of the fillers (Fig. S.7) were used to determine their flake size distribution (Fig. S.8).

It has been reported that acid treatment drastically changes the octahedral and tetrahedral crystalline structures of Verm and results in the formation of amorphous silica [33], as confirmed by the decrease in intensity and broadening of the peaks in the XRD spectra of SN, functionalized SN and exfoliated SN, as compared to those of layered precursor Verm (Fig. 3 a). The characteristic diffraction peaks of Verm appear at 6.39° (d-spacing = 1.38 nm, 002), 12.27° (d-spacing = 0.72 nm, 004), 18.93° (d-spacing = 0.47 nm, 006), and 25.35° (d-spacing = 0.35 nm, 008). These changes in the structure are also confirmed by the lower intensity of the Si–O stretching peak (at 650 cm^{-1}) in the FTIR spectra of the fillers (Fig. 3 b) [16]. The band at 980 cm^{-1} indicates the Si–O bonds stretching vibration of Verm. New bands at 800 and 1060 cm^{-1} originate from bending vibration and stretching of amorphous Si–O bonds [34] and the band at 960 cm^{-1} is assigned to the acid leaching of Mg^{2+} and Al^{3+} cations from the crystal structures of Verm and formation of Si–OH groups [34]. However, the FTIR spectrum does not show peaks related to sulfonic groups (at 1235-1145 cm^{-1} [35]) for S-SN and amine groups (at 3455 and 1636 cm^{-1} [36,37]) for N-SN. The

large peak of SiO$_4$ tetrahedral at 1060 cm^{-1} may overlap with the sulfonic peak [38], while OH vibration (OH-stretching vibration at around 3400 cm^{-1} and OH-bending vibration at 1654 cm^{-1}) can overlap with the amine peak [39].

The thermal stability of Verm and all the prepared fillers were studied by TGA and the curves are presented in Fig. S.9. Compared to SN, the lower weight loss of Verm can be attributed to the lack of functional groups and the higher heat resistance of the exposed silica in Verm [16].

The surface composition and functional groups of Verm and the fillers were studied by XPS, and the survey spectra are shown in Fig. 3 c. For Verm, the main characteristic peaks correspond to Si, O, Al and Mg elements, in accordance with its chemical formula. Because the majority of Al and Mg cations in Verm are dissolved during the acid-treatment reaction, the intensities of Mg and Al peaks are smaller for the SN. The C peaks in all survey spectra are ascribed to the surface-absorbed carbon-based contaminants [40]. Furthermore, the XPS survey spectra of S-SN and N-SN contain S and N peaks, respectively, which confirms the presence of sulphur and nitrogen elements in S-SN and N-SN at very low concentrations (atomic percentages of N and S are 3.29 and 6.04%, respectively). Further analyses of the functional groups are carried out by the high-resolution S 2p and N 1s XPS spectra of S-SN and N-SN (Fig. S.10 a&b). In addition, to confirm that the hydroxyl groups are present in the fillers, the high-resolution O 1s XPS spectra of all samples are shown in Fig. S.11. The amount of Si–OH groups increases from 0 wt % for Verm to 2.6 wt%, 1.69 wt% and 1.44 wt% for SN, S-SN and N-SN, respectively, which is consistent with the presence of the new band at 960 cm^{-1} in the FTIR results (Fig. 3 b). More fillers' characterization including TEM can be found in a previously published work [16].

3.2. Membrane characterization

TGA curves of neat PIM-1 and selected membranes containing SN-based fillers are shown in Fig. 4 a. All the membranes are stable until 460 °C due to the dipolar interaction in nitrile groups. The main weight loss occurs from 460 to 800 °C, which is assigned to the ether linkage
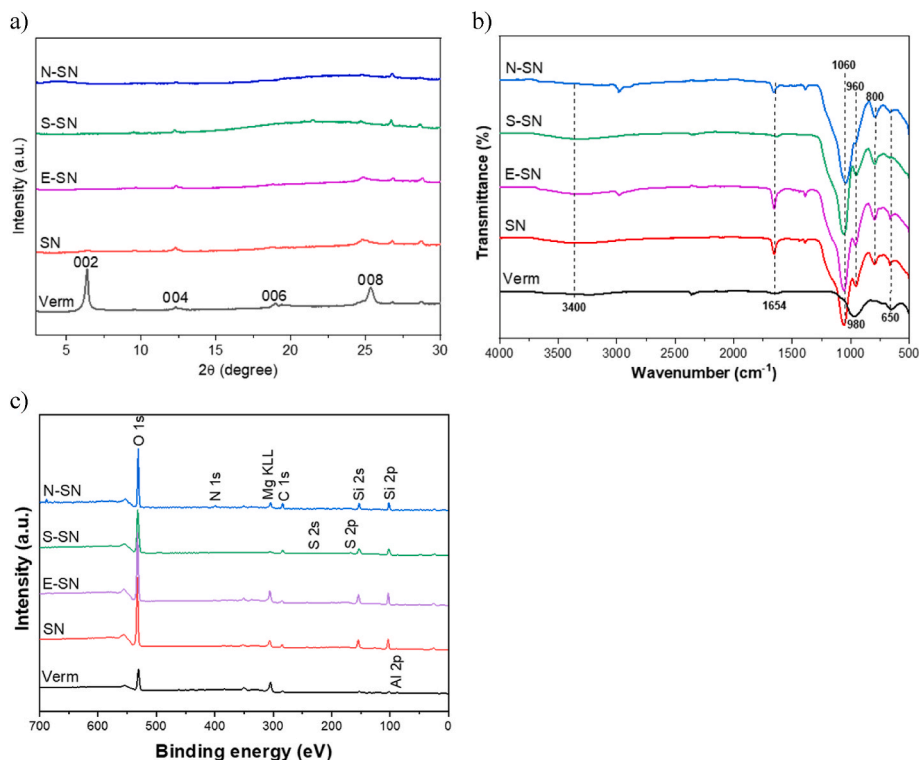

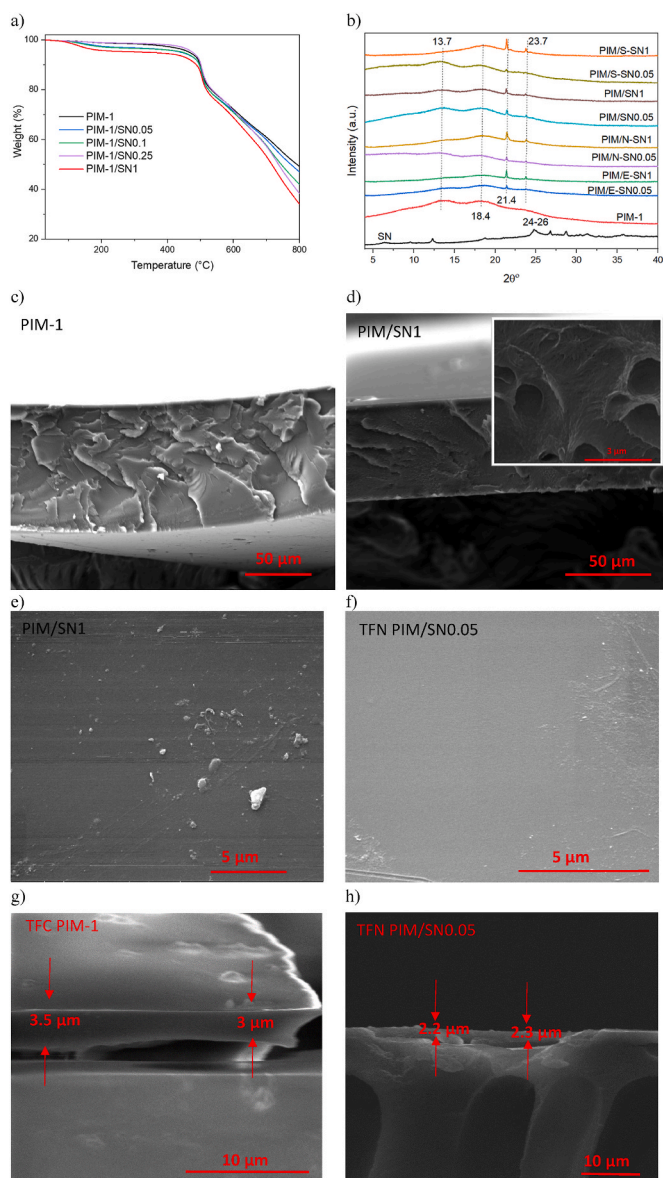**Fig. 3.** XRD patterns (a), FTIR spectra (b), and XPS spectra (c) for Verm, SN, E-SN, S-SN and N-SN.

Fig. 4. TGA curves (a) and XRD patterns (b) of PIM-1 and selected MMMs. Cross-sectional SEM image of thick PIM-1 and PIM/SN1 membranes (c & d), surface SEM image of PIM/SN1 and TFN PIM/SN0.05 (e & f). Cross-sectional SEM image of TFC PIM-1 and TFN PIM/SN0.05 (g & h).

removal of PIM-1 polymer [11]. Also, the small weight loss (<4 wt%) up to 200 °C is due to the removal of adsorbed water and organic solvents used in the PIM-1 synthesis and membrane fabrication process.

The XRD spectra of neat PIM-1 and selected MMMs containing 0.05 and 1 wt% of fillers are shown in Fig. 4 b. The two broad peaks at 13.7° and 18.4°, which are present in all spectra, correspond to the PIM-1 micropores created by the contorted ladder backbone structure and the chain-to-chain distance of the space-packed polymer matrix, respectively [41]. For the MMMs, the peaks at 21.4° and 23.7° arise from the filler and their intensities increase by increasing the filler concentration. These two peaks correspond to the small SN peaks at 21.4° and the relative wide peak at 24–26° (Fig. 3 a). It seems that by incorporating the fillers in the polymer matrix, the SN peak at 24–26° moves towards a lower 2θ value (23.7°). In addition, by increasing the filler's concentration the intensity of the first PIM-1 peak (13.7°) decreased. These can be justified by the interrupted chain packing of the polymer due to the presence of the fillers [42,43], intercalation of PIM-1 polymer chains between the filler interlayer [44], and the rearrangement of PIM-1

chains as a consequence of the possible hydrogen bonding between PIM-1 and the fillers. It has been reported that the functional groups (-OH, –SO$_3$H, –NH$_2$) in the fillers can form hydrogen bonds with cyano (-C $\equiv$ N) and ether (-O-) groups in the PIM-1, giving rise to FTIR peaks with decreased intensity and wavenumber shifting [45–47]. However, as seen in Fig. S.12, the FTIR spectra of the MMMs do not show any alterations with respect to that of a neat PIM-1 membrane, possibly due to the very low concentration of the fillers.

The cross-sectional SEM images of neat PIM-1 and PIM/SN1 are shown in Fig. 4 c&d, respectively. No visible agglomeration of the filler is observed (a higher magnification SEM image is shown as an inset in Fig. 4 d). The polymer veins and wrinkles seen on the cross-sectional images are due to the membrane fracturing method. The surface SEM images of thick freestanding PIM/SN1 and TFN PIM/SN0.05 membranes are shown in Fig. 4 e&f. In some cases (i.e. PIM/S-SN1, Fig. 4 e), pinholes (depth less than 100 nm) appeared on the surface of the membrane as a consequence of rapid evaporation of chloroform (low boiling point solvent) during membrane formation [48]. The cross-sectional SEM images of TFC PIM-1 and TFN/SN0.5 are shown in Fig. 4 g&h. The thicknesses of TFC and TFN membranes were in the range of 2–3.5 μm. The cross-sectional and surface SEM images of other thin film and freestanding membranes are shown in Fig. S.13. To convert permeance to permeability (equation (11)) the average PIM-1 thickness was considered 2.5 μm. It should be noted that the SEM images show only a small section of the membrane, but thickness values were very similar in all observed samples (2 samples for each membrane variant).

3.3. Gas separation results

3.3.1. Thick membranes

The freestanding membranes were tested one day after preparation for the separation of binary gas mixtures of CO$_2$/CH$_4$ and CO$_2$/N$_2$ (1:1, v:v). At least 3 coupons of each membrane variant were tested, and the average results and standard deviation are reported (Table S.3). The gas permeability values are plotted in Fig. 5 a and b, where it can be seen that CO$_2$ is the highest permeating gas and N$_2$ the slowest permeating gas. Therefore, CO$_2$/N$_2$ selectivity is higher than CO$_2$/CH$_4$ selectivity.

Filler morphology plays an important role in membrane performance. For instance, in the work by Althumayri et al. [49], a maximum gas permeability was achieved for PIM-1-based MMMs containing very low concentrations of high aspect ratio sheet-shaped fillers (graphene, 0.001 wt%), as compared to the concentration that was needed to observe a similar increase when spherical filler were used (fumed silica, 24 wt%). Similarly, the addition of high aspect ratio SN into PIM-1 in this work leads to a noticeable improvement in CO$_2$ permeability with only 0.05 wt% of filler. As seen in Fig. 5a, all the MMMs containing 0.05 wt% of filler show a higher CO$_2$ permeability than the neat PIM-1 membrane; PIM/S-SN (9014 $\pm$ 47 Barrer), PIM/N-SN (8252$\pm$ 1186 Barrer), PIM/E-SN (7825$\pm$ 928 Barrer), PIM/SN (7312$\pm$ 1037 Barrer) > neat PIM-1 (6411$\pm$ 868 Barrer). In Fig. 5b (CO$_2$/N$_2$ separation), the same CO$_2$ permeability trend can be observed with higher permeabilities for the low fillers concentration. The widely-accepted gas transport mechanism in PIM-1 membranes is solution-diffusion. In polymer membranes, gas permeability can increase if the solubility and/or the diffusivity terms increase as a result of structural or chemical modifications. In MMMs, the addition of fillers can disrupt polymer chain packing and result in an increase in the free volume of the membranes (as indicated by the XRD results) [50] and thus an increase in the diffusion coefficient of penetrant gas [51]. Furthermore, the pores of the fillers can lead to additional gas transport pathways (if the mesopores are interconnected) [15]. With the addition of the fillers at low loadings, the permeability enhancement for condensable gases (CO$_2$ and CH$_4$) is larger than for non-condensable N$_2$ and thus, the CO$_2$/N$_2$ selectivities improve more than CO$_2$/CH$_4$ selectivity; for instance, CO$_2$/CH$_4$ and CO$_2$/N$_2$ selectivities increase from 11.5 to 18.7 for neat PIM-1 to 11.8 and 22, respectively for PIM/S-SN0.05. The same behaviour has been
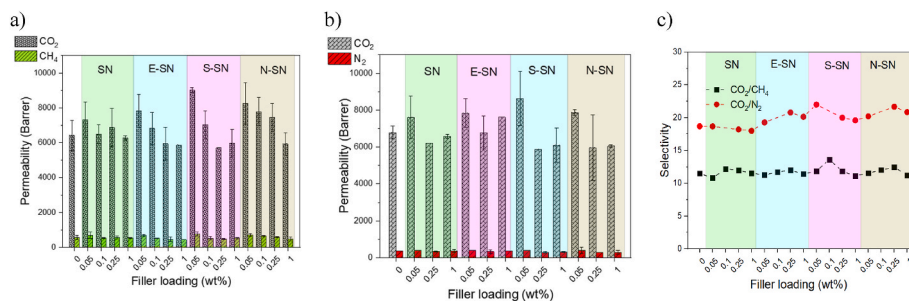
Fig. 5. Effect of filler loading on permeability (a, b) and selectivity (c) of fresh membranes for CO_2/CH_4 and CO_2/N_2 separation. MMMs containing 0.1 wt% fillers were not tested for CO_2/N_2 separation due to time constraints.

reported in the literature by using silica NPs as a filler, ascribing the selectivity enhancement to the interaction between the –OH groups of silica NPs and gases with polar bonds such as CO_2 and also modification of polymer chain structure [52,53]. The synthesized layered SN possesses more hydroxyl groups that can enhance the interactions with penetrant molecules, as compared to other silica NPs and silica nanoclusters [16].

It was expected that, unlike 2D impermeable fillers, mesoporous SN fillers could provide extra pathways and increase the CO_2 permeability at all filler loadings. However, by increasing the loading up to 1 wt%, the CO_2 permeability for all MMMs decreased to lower values than that of the neat PIM-1, same behaviours as the one observed in other studies with GO derivatives and boron nitride [2,11,12]. Therefore, this suggests that the either the fillers' mesoporosity is not interconnected or the polymer chains are blocking the pores, or both. Moreover, some other factors such as the orientation of pores contribute to the performance of the MMMs. It has been reported that fast evaporation of PIM-1 solvent (chloroform) from casting solution makes shear forces that arrange nanofillers vertically which makes the pores of the filler inaccessible for gas transport [54]. It should be noted that the BET surface area of the fillers is lower than that of PIM-1 (Table S.2 and Fig. S.6) and higher filler concentrations can decrease access to the polymer porosity, increase tortuosity and induce rigidification of polymer chains, thus reducing polymer chain mobility and membrane permeability.

Another parameter that can affect the performance of the MMMs is the filler lateral flake size. Shen et al. [55] studied the effect of the lateral flake size of GO (ranging from 100 nm to 10 μm) on the CO_2 separation performance of polyether block amide (PEBA) MMMs. They showed that the addition of 0.1 wt% of GO flakes with an average lateral size of 1–2 μm induced the highest CO_2 permeability (110 Barrer) compared to MMMs that contained smaller or larger flakes. This was attributed to an optimum tuned polymer chains mobility caused by the medium-sized GO nanosheets. The average lateral flake size of S-SN and N-SN fillers in this work is 0.35 ± 0.22 and 0.33 ± 0.22 μm, respectively (Table S.2). These values lie in between those for SN and E-SN (0.55 ± 0.34 and 0.28 ± 0.17, respectively), inducing perhaps the aforementioned optimum polymer chain mobility at loadings of 0.05 wt% of filler and leading to the observed higher CO_2 permeabilities of such PIM/S-SN and PIM/N-SN membranes.

The presence of some branched PIM-1 structures is confirmed by NMR. These structures with -OH groups at the branch points contribute to improving the interaction with the fillers [12]. The fillers and the polymer chains show good compatibility and interfacial voids did not form, also all the MMMs, regardless of the fillers loading, have almost the same or higher selectivities than the neat PIM-1 membrane. Compared with PIM/SN MMMs, the higher selectivities of PIM/E-SN, PIM/S-SN and PIM/N-SN MMMs can be attributed to the higher compatibility of the filler and polymer matrix due to the functionalization and smaller size [15]. EDS was carried out on selected cross sections of PIM/SN1 and PIM/S-SN1 membranes, and mappings of carbon (C), oxygen (O), and silicon (Si) elements are shown in Fig. S.14 a&b in the

supporting information. Si is only present in the fillers and thus, the observed even distribution of this element for both cross sections indicate homogenous distribution of the fillers in the membranes. Moreover, the selectivity enhancement due to the introduction of polar sulfonic acid and amine groups into membranes has been reported elsewhere [2, 11,21,56,57]. This enhancement may not be noticeable in this study due to the small concentration of filler in the MMMs and the low percentage of organic functional groups in the filler. MMMs with higher filler loadings (up to 5 wt%) were prepared but filler agglomeration on the surface could be observed. Single gas measurements were carried out on a constant volume-variable pressure instrument to calculate the solubility (*S*) and diffusivity (*D*) coefficients of the membranes (values shown in Table 1) and the results are discussed in next paragraphs.

The aged membranes were retested after 45, 110 and 150 days for CO_2/CH_4 separation and the new permeability and selectivity values are shown in Table S.3. Some of the aged membranes showed defects probably due to loading/unloading into the gas separation cell several times; for some membranes, only one sample survived at the end of the aging period and therefore standard deviation is not reported for them.

Physical aging decreases the fractional free volume of the membranes and improves their sieving ability, as confirmed by the lower CO_2 and CH_4 permeabilities and higher CO_2/CH_4 selectivity as compared to fresh membranes. The CO_2 permeability drop for neat PIM-1 and the MMMs containing 0.05 and 1 wt% of the fillers has been calculated by equation (5) and the results are compared in Fig. 6 a. The permeability drop is more pronounced during the first 45 days of aging followed by a gradual decrease. After 150 days, the majority of the MMMs (all except those containing 0.05 wt% of sulfonic acid and amine-functionalized SN, PIM/S-SN0.05 and PIM/N-SN0.05) showed lower CO_2 permeability drop compared with neat PIM-1 membrane. Nevertheless, all the 150 days-aged MMMs had higher CO_2 permeability (Fig. 6 b) and relative CO_2 permeability (values shown in Table S.3). In addition, by increasing the filler concentration the permeability drop decreased by ~50% in all cases which is attributed to rigidification effects of the fillers [58]. At 1 wt% of the fillers, the permeability drop at day 150 is: neat PIM-1 (4011 Barrer) > PIM/E-SN (2124 Barrer) = PIM/N-SN (2124 Barrer) > PIM/S-SN (1883 Barrer).

For gases such as H_2, CO_2, N_2 and CH_4, PIM-1 membranes have higher solubility coefficients than other high free volume polymer membranes such as PTMSP [59]. This is caused by the presence of polar cyano groups in PIM-1 that favours sorption [60]. The *D* and *S* values of 180 days-aged PIM/SN, PIM/S-SN, PIM/N-SN and neat PIM-1 membranes were calculated from single gas CO_2 and CH_4 permeation experiments in a time-lag set-up and the results are reported in Table 1. Just one sample of each membrane was tested since the obtained gas permeability results had no significant deviations from values acquired with the GC-equipped system for gas-mixtures. Both *D* and *S* values for CO_2 are larger than those for CH_4 for all neat and SN-containing PIM-1 membranes due to the smaller kinetic diameter of CO_2 and its higher polarity. It has been reported that aging has a dramatic effect on the diffusivity of PIM-1 membranes, but not so much on the solubility [61].
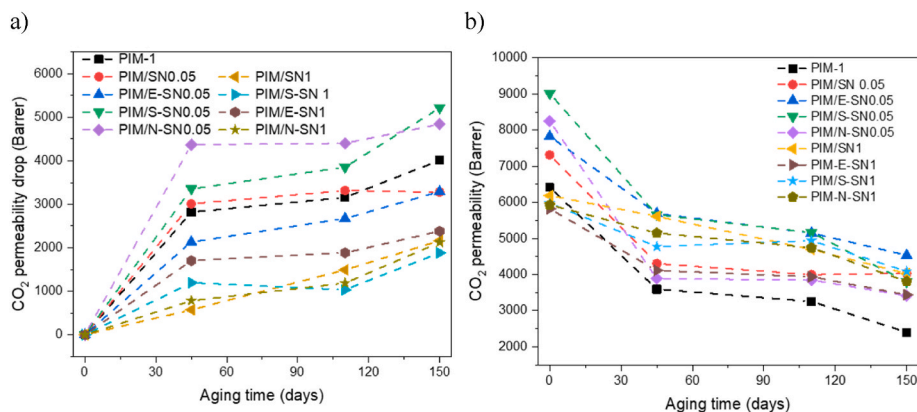
Fig. 6. Physical aging of neat PIM and MMMs containing 0.05 wt% and 1 wt% of fillers. CO_2 permeability drop vs time (a), and CO_2 permeability vs time (b).

Table 1

CO_2 and CH_4 permeability (*P*, Barrer), diffusion coefficient (*D*, $cm^2 s^{-1}$), solubility parameter (*S*, cm^3 (STP) $cm^{-3}.cmHg^{-1}$), CO_2/CH_4 ideal selectivity, solubility selectivity and diffusion selectivity of PIM-1 and MMMs after 180 days of aging.

Membrane	*P*		*D* ($\times 10^7$)		*S* ($\times 10^3$)		ideal selectivity	$\dfrac{S_{CO_2}}{S_{CH_4}}$	$\dfrac{D_{CO_2}}{D_{CH_4}}$
	CO_2	CH_4	CO_2	CH_4	CO_2	CH_4			
PIM-1	2267	110	11.25	1.763	201.5	62.17	20.7	3.2	6.4
PIM/SN0.1	4138	232	18.15	1.793	228.0	129.4	17.8	1.7	10.1
PIM/SN1	4657	228	17.82	1.731	261.3	131.7	20.4	2.0	10.3
PIM/N-SN0.1	4410	283	10.76	1.647	410.0	171.6	15.6	2.4	6.5
PIM/N-SN1	4812	208	13.90	1.164	346.2	178.9	23.1	1.9	11.9
PIM/S-SN0.1	3275	214	12.82	1.317	255.6	162.3	15.3	1.6	9.7
PIM/S-SN1	4620	247	17.65	2.583	261.7	95.74	18.7	2.7	6.8

For the prepared MMMs in this work, gas diffusivities are larger as compared to those of the neat PIM-1, indicating that the presence of fillers leads to higher free volume after prolonged aging. Moreover, MMMs containing 0.1 and 1 wt% of fillers show higher solubility values than PIM-1, which suggest more sorption sites in the MMMs that can increase gas permeability. It is also worth noting that the incorporation of high-aspect-ratio SN increases the gas diffusivity selectivity, as the diffusion of CH_4 (larger gas molecules) is more restricted than the diffusion of CO_2 (smaller molecules). This behaviour is in agreement with the reported performance of GO-containing MMMs reported by Li et al. [54].

3.3.2. Thin film membranes

The CO_2/CH_4 separation performance of fresh and aged (7 and 28 days) TFC PIM-1 and TFN membranes are shown in Fig. 7 a. It should be noted that the support was highly porous and had a CO_2 permeance of 10^5 GPU [6], also no significant penetration of PIM-1 solution into the support was observed. The CO_2 permeances of the TFN membranes containing 0.05 wt% S-SN (3771 ± 57 GPU), N-SN (2956 ± 602 GPU), and SN (2864 ± 260 GPU) are higher than that of TFC PIM-1 (2778 ± 1010 GPU), however, the permeance of TFN PIM/E-SN (1847 ± 848 GPU) is lower. It seems that the exfoliated SN (E-SN) can partially block PIM-1 pores, decreasing the permeance and increasing the selectivity. Among the prepared thin film membranes, PIM/E-SN has the highest initial selectivity (9.3) and TFN PIM/S-SN0.05 has the highest permeance. The CO_2 permeances in this study (thickness = 2.5 μm) are lower than the values reported by Foster et al. [6,30] which can be attributed to the thinner PIM-1 layer (<2 μm) and different PIM-1 topology.

In all the prepared TFNs, both CO_2 permeance and selectivity decreased after 28 days. However, different trends in CO_2/CH_4 selectivity are observed; the CO_2/CH_4 selectivity in the neat PIM-1 and the TFN containing 0.05 wt% SN is almost constant over time, for TFNs PIM/S-SN0.05 and PIM/N-SN0.05 there is a maximum value for

selectivity at day 7, and for TFN PIM/E-SN0.05, the selectivity continuously decreases with time. Foster et al. [6] also reported different aging behaviour for TFC PIM-1 membranes due to the different polymer topologies and network content, however, after 28 days, in almost all cases the permeance and selectivity of membranes decreased significantly compared to the fresh membranes.

The relative CO_2 permeance versus time for freestanding PIM-1, TFC PIM-1, and TFN membranes are compared in a semi-log plot (Fig. 7 b). Because freestanding PIM/S-SN1 showed the lowest permeability drop among freestanding membranes, TFN PIM/S-SN membranes at filler loadings of 0.25 and 1 wt% were also fabricated. Like freestanding membranes, CO_2 permeance decreased by increasing S-SN loading from 0.05 wt% (3771 ± 57 GPU) to 0.25 wt% (2755 ± 910 Barrer). The membrane at 1 wt% of S-SN had defects due to possible agglomeration of the fillers, and was not selective. As seen in Fig. 7 b, TFN PIM/S-SN0.05, TFN PIM/S-SN0.25 and TFN PIM/N-SN0.05 showed almost the same aging behaviour, and after 28 days, the corresponding relative CO_2 (%) permeances were 11, 14 and 13%, respectively. For TFC PIM-1 and TFN PIM/E-SN0.05 the permeance dropped by 97% and 98%, respectively. This shows the positive effect of S-SN and N-SN to slow down physical aging. The gas separation performances of fresh and aged thin membranes are mentioned in Table S.4.

3.3.3. Robeson upper-bound and comparison with values in the literature

The gas separation performance for the CO_2/CH_4 mixture with the prepared thin and thick membranes is plotted in a Robeson upper-bound diagram [4] in Fig. 8. To convert permeance values of the thin films into permeabilities for the Robeson plot, a thickness of the selective layers of 2.5 μm (obtained by the cross-sectional SEM images) was assumed.

The incorporation of 0.05 wt% E-SN, S-SN and N-SN into freestanding PIM-1 matrices is an effective strategy to surpass the 2008 upper bound for fresh membranes. After 150 days, all the thick membranes (neat PIM-1 and the MMMs) follow the upper bound towards higher selectivities and lower permeabilities, as expected. Moreover, the
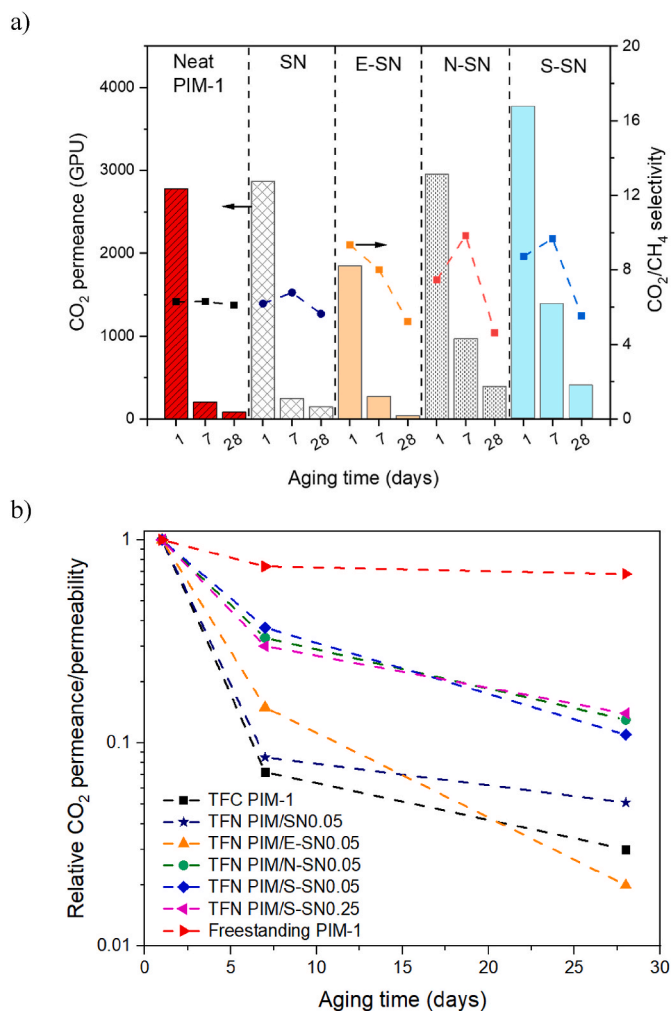
a)

b)

Fig. 7. CO_2 permeance and CO_2/CH_4 selectivity for fresh and aged TFC PIM-1 and TFN membranes containing 0.05 wt% fillers (a). Semi-log plot of the relative CO_2 permeance/permeability versus time for thick PIM-1, TFC PIM-1 and TFN membranes (b).
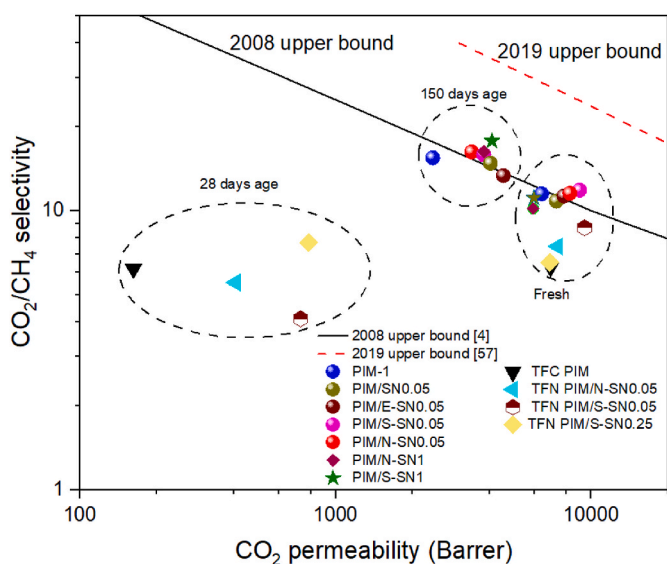

Fig. 8. Robeson upper bound plot for CO_2/CH_4 separation of thick and TFC PIM-1, TFNs and MMMs containing 0.05 wt% of the fillers, and TFN/S-SN0.25 membranes.

MMMs containing 1 wt% of S-SN and N-SN remain closer to the initial permeability values, indicating lower rates of physical aging as discussed in section 3.3.1 and after 150 days their performance is above the 2008 upper bound.

Among the thin film membranes, TFN PIM/S-SN0.05 exhibits the best initial performance as it is nearer the 2008 upper bound and after 28 days, similarly to thick membranes, the TFNs showed a lower permeability drop than the TFC PIM-1 membrane.

The CO_2/N_2 separation performances of fresh freestanding membranes and the 2008 Robeson upper bound are shown in Fig. S.15. PIM-1 gas separation performance for this mixture lies at the 2008 upper bound and the MMMs with 0.05 wt% of fillers are above the upper bound. Moreover, the PIM-1/S-SN0.05 membrane is closer to the 2019 upper bound proposed by McKeown et al. [62].

The CO_2/CH_4 separation performances of some of the fresh and aged membranes prepared in this study are compared with other data from the literature in Table 2. The aging behaviour of the pristine PIM-1 membrane in this work is similar to the one reported in the work by Alberto et al. [2]. However, the permeability drop due to physical aging is higher than the one reported by Ameen et al. [12] for PIM-1. The difference in aging is assigned to the difference in polymer structure and membrane storage conditions. It is found that the PIM-1 membranes with more branched structures experience slower physical aging [30].

Porous silicalite-1 (390 $m^2 g^{-1}$) with MFI structure [63], nonporous fumed silica NPs [64,65] and methyl functionalized fumed silica (DMBA-NP) [15], have been used as fillers in freestanding PIM-1-based membranes for CO_2/CH_4 or CO_2/N_2 separations (Table 2), but some of these works lack evaluation of aging [63,64]. By adding fumed silica [64] and DMBA-NP [15] to PIM-1, the permeability increased while the selectivity was compromised. The same behaviour was observed by incorporating fumed silica into thermal-oxidatively crosslinked PIM-1 (TOX-PIM-1) [65]. This was explained by the polymer chain rearrangement when fillers were added; higher D values of the MMMs compared with the neat PIM-1, and interfacial voids due to poor interaction between the filler and PIM-1 chain. However, in our work, the MMMs showed higher permeability (at low fillers loadings) than the pure PIM-1 membranes, without any sacrifice in their selectivity.

The spin-lattice relaxation time (T_1) measured by ^{13}C NMR was employed to probe the relative mobility of carbon sites of PIM-1 after the addition of porous aromatic framework (PAF) [66] and DMBA-NP [15]. In both cases, the mobility of carbon atoms decreased over time and aging was improved. PIM-1/PAF and PIM-1/DMBA-NP membranes lost around 6 wt% of their initial permeability after 240 days and 60 days, respectively (Table 2). However, the initial performances of both membranes were below the 2008 Robeson upper bound.

Kinoshita et al. [7] studied the aging of 2.5-μm-thick thin films of PIM-1 and TFNs containing 5 wt% of amino POSS (OAPS). Both membranes lost ~90% of their initial permeability after 1 month; the aged membranes had a permeability of ~600 Barrer (Table 2). This is similar to the loss percentage experienced by the TFNs containing 0.05 wt% of S-SN in our work for the same aging period. However, our membranes showed a permeability of ~1000 Barrer, 5 times higher than that of our 28-days-aged pristine PIM-1 TFC. In another study by Foster et al. [6], 1-month-aged PIM-1 thin films containing 20 wt% of a high network content PIM-1 sample showed an impressive CO_2 permeability of 3480 GPU (~7000 Barrer) that went down to only 34.9 GPU (70 Barrer) after 4 months of aging. This suggests delayed aging in early stages for TFC membranes containing high-free volume polymer-based fillers, that unfortunately ends in poor longer term performance due to molecular relaxation.

Bhavsar et al. [67] employed a carbonized form of hypercrosslinked polystyrene (C-HCP) as a nanofiller in PIM-1 TFC membranes that led to an increase in CO_2 permeability from 6662 Barrer for TFC PIM-1 (~2 μm) to 1110^4 Barrer for TFN PIM-1/C-HCP (40 wt%, ~7 μm). This is the highest permeability reported to date, yet the aging effect is quite severe; 90-days-aged pristine and nanocomposite membranes lost 90 and

Table 2
CO_2/CH_4 and CO_2/N_2 separation performance in this work and in the literature.

Membrane	Day	CO_2 permeability (Barrer)	Selectivity		Ref
			CO_2/CH_4	CO_2/N_2	
PIM-1	0	6411	11.5	18.6	This work
	150	2400	15.5	–	
PIM/S-SN0.05	0	9014	11.9	22	This work
	150	3800	15.9	–	
PIM/S-SN1	0	5972	11.1	19.6	This work
	150	4088	17.8	–	
TFC PIM-1 (2.5 μm)	0	6945	6.3	–	This work
	28	202	6.1	–	
TFN PIM/S-SN0.05 (2.5 μm)	0	9427	7.4	–	This work
	28	1007	4.6	–	
TFN PIM/S-SN0.25 (2.5 μm)	0	6887	6.5	–	This work
	28	965	7.7	–	
PIM-1	0	6400	20.3	–	[2]
	155	2000	30	–	
PIM-1	0	6000	–	15	[64]
PIM-1/fumed silica (13 v %)		10100		12	
PIM/GO-POSS (0.75)	0	4462	13.7	20.1	[51]
	160	3301	15.9	–	
PIM-1/PAF (10 wt%)	0	10500	–	15	[66]
	240	9700		20	
PIM-1/DMBA-NP (15 wt %)	0	6200	–	–	[15]
	60	5900	–	–	
PIM-1/silicalite-1 (35 v %)	0	2530	13.8	30	[63]
PIM-1	0	5040	17.5	20.6	[65]
PIM-1/fumed silica (5 wt %)		6061	14.2	18.3	
TOX-PIM-1		1104	69.2	36.6	
TOX-PIM-1/fumed silica (5 wt%)	0	1824	55	29.8	
	740	400	56	–	
PIM-1/OAPS (5 wt%), (2.5 μm)	0	3811	12.6	16.6	[7]
	90	2384	17	–	
TFC PIM-1 (2.5 μm)	0	6007	8.7	15.6	
	30	660	–	27	
TFN PIM/OAPS (5 w.t %), (2.5 μm)	0	5345	10.6	19.4	
	30	641	–	25	
TFC PIM-1 (1.7 μm)	0	11010	–	13.7	[30]
	28	802		11	
TFN PIM-1/colloidal network- rich filler (20 wt%), (2 μm)	0	11800	–	16.6	[6]
	28	6960		14.9	
	130	70		10.7	
TFC PIM-1 (2 μm)	0	9356	–	11.2	
	28	268		3.5	
TFC PIM-1 (2 μm)	0	6662	–	14.2	[67]
	90	776		24.5	
TFN PIM-1/C-HCP (40 wt%), (7 μm)	0	11×10^4		9.2	
	90	19600		13.5	

95% of their initial permeability, respectively.

4. Conclusions

Porous silica nanosheets (SN), exfoliated SN, amine and sulfonated SN were used as fillers in freestanding membranes and thin films of PIM-1, and the CO_2/CH_4 and CO_2/N_2 separation performance of the membranes was studied over 5 months. The fillers had good compatibility with PIM-1 and their incorporation was an efficient strategy to boost the initial gas permeability and suppress physical aging. By incorporating 0.05 wt% SN and surface modified SN (S-SN and N-SN) into the PIM-1 polymer, the permeabilities of both freestanding and TFN membranes increased compared to neat PIM-1 membrane, without any sacrifice in the selectivity. For instance, compared to the pure PIM-1, the MMMs containing 0.05 wt% of S-SN showed a 40% higher CO_2 permeability, and 22% enhancement in CO_2/N_2 selectivity. In addition, using functionalized SNs as fillers at high loadings ($>$0.05 wt% for freestanding membranes and 0.05 and 0.25 wt% for thin films) can slow down physical aging. 150-days-aged freestanding PIM/SN1 and 28-days-aged

TFN PIM/S-SN0.05 showed 70% and 5 times higher CO_2 permeability than the pure thick PIM-1 and TFC PIM-1 membranes, respectively.

Although physical aging of PIM-1 membranes can be slowed down with the addition of fillers (lower rate of gas permeability drop over time for MMMs), thin films still dramatically lose gas permeability in just a few weeks. Therefore, more research is needed in order to find more efficient fillers or alternative ways of freezing the PIM-1 structure for a more predictable and stable gas separation performance over time.

CRediT authorship contribution statement

Sajjad Mohsenpour: Conceptualization, Investigation, Methodology, Formal analysis, Visualization, Writing – original draft. **Zunmin Guo:** Conceptualization, Investigation, Methodology, Formal analysis, Writing – review & editing. **Faiz Almansour:** Methodology. **Stuart M. Holmes:** Supervision, Funding acquisition. **Peter M. Budd:** Supervision, Writing – review & editing. **Patricia Gorgojo:** Supervision, Project administration, Funding acquisition, Writing – review & editing.

Declaration of competing interest

The authors declare that they have no known competing financial interests or personal relationships that could have appeared to influence the work reported in this paper.

Data availability

Data will be made available on request.

Acknowledgments

Appendix A. Supplementary data

Supplementary data to this article can be found online at https://doi.org/10.1016/j.memsci.2022.120889.

References

[1] Y. Zhang, et al., Current status and development of membranes for CO_2/CH_4 separation: a review, Int. J. Greenh. Gas Control 12 (2013) 84–107.

[2] M. Alberto, et al., Impeded physical aging in PIM-1 membranes containing graphene-like fillers, J. Membr. Sci. 563 (2018) 513–520.

[3] P.M. Budd, et al., Polymers of intrinsic microporosity (PIMs): robust, solution-processable, organic nanoporous materials, Chem. Commun. (2) (2004) 230–231.

[4] L.M. Robeson, The upper bound revisited, J. Membr. Sci. 320 (1–2) (2008) 390–400.

[5] Z.-X. Low, et al., Gas permeation properties, physical aging, and its mitigation in high free volume glassy polymers, Chem. Rev. 118 (12) (2018) 5871–5911.

[6] A.B. Foster, et al., Importance of small loops within PIM-1 topology on gas separation selectivity in thin film composite membranes, J. Mater. Chem. 9 (38) (2021) 21807–21823.

[7] Y. Kinoshita, et al., Enhanced PIM-1 membrane gas separation selectivity through efficient dispersion of functionalized POSS fillers, J. Membr. Sci. 539 (2017) 178–186.

[8] Q. Song, et al., Controlled thermal oxidative crosslinking of polymers of intrinsic microporosity towards tunable molecular sieve membranes, Nat. Commun. 5 (1) (2014) 1–12.

[9] F.Y. Li, et al., High-performance thermally self-cross-linked polymer of intrinsic microporosity (PIM-1) membranes for energy development, Macromolecules 45 (3) (2012) 1427–1437.

[10] N. Tien-Binh, D. Rodrigue, S. Kaliaguine, In-situ cross interface linking of PIM-1 polymer and UiO-66-NH2 for outstanding gas separation and physical aging control, J. Membr. Sci. 548 (2018) 429–438.

[11] J.M. Luque-Alled, et al., Gas separation performance of MMMs containing (PIM-1)-functionalized GO derivatives, J. Membr. Sci. 623 (2021), 118902.

[12] A.W. Ameen, et al., 2D boron nitride nanosheets in PIM-1 membranes for CO_2/CH_4 separation, J. Membr. Sci. (2021), 119527.

[13] S. Pavlidou, C. Papaspyrides, A review on polymer–layered silicate nanocomposites, Prog. Polym. Sci. 33 (12) (2008) 1119–1198.

[14] P. Goh, et al., Recent advances of inorganic fillers in mixed matrix membrane for gas separation, Separ. Purif. Technol. 81 (3) (2011) 243–264.

[15] N. Sakaguchi, et al., Superhigh CO_2-permeable mixed matrix membranes composed of a polymer of intrinsic microporosity (PIM-1) and surface-modified silica nanoparticles, ACS Appl. Poly. Mater. 1 (9) (2019) 2516–2524.

[16] Z. Guo, et al., High-performance polymer electrolyte membranes incorporated with 2D silica nanosheets in high-temperature proton exchange membrane fuel cells, J. Energy Chem. 64 (2022) 323–334.

[17] D. Liu, et al., Fast and high adsorption of Ni (II) on vermiculite-based nanoscale hydrated zirconium oxides, Chem. Eng. J. 360 (2019) 1150–1157.

[18] R.K. Gogoi, K. Raidongia, Intercalating cation specific self-repairing of vermiculite nanofluidic membrane, J. Mater. Chem. 6 (44) (2018) 21990–21998.

[19] Q. Ma, et al., Bio-inspired stable lithium-metal anodes by co-depositing lithium with a 2D vermiculite shuttle, Angew. Chem. Int. Ed. 58 (19) (2019) 6200–6206.

[20] S.H. Pang, et al., PIM-1 as a solution-processable "molecular basket" for CO2 capture from dilute sources, ACS Macro Lett. 4 (12) (2015) 1415–1419.

[21] A.L. Khan, et al., Mixed matrix membranes comprising of Matrimid and–SO_3H functionalized mesoporous MCM-41 for gas separation, J. Membr. Sci. 447 (2013) 73–79.

[22] M. Tamaddondar, et al., Intrinsically microporous polymer nanosheets for high-performance gas separation membranes, Macromol. Rapid Commun. 41 (2) (2020), 1900572.

[23] F.C. Moura, R.M. Lago, Catalytic growth of carbon nanotubes and nanofibers on vermiculite to produce floatable hydrophobic "nanosponges" for oil spill remediation, Appl. Catal. B Environ. 90 (3–4) (2009) 436–440.

[24] C. Prapainainar, et al., Surface modification of mordenite in Nafion composite membrane for direct ethanol fuel cell and its characterizations: effect of types of silane coupling agent, J. Environ. Chem. Eng. 4 (3) (2016) 2637–2646.

[25] T. Emmler, et al., Free volume investigation of polymers of intrinsic microporosity (PIMs): PIM-1 and PIM1 copolymers incorporating ethanoanthracene units, Macromolecules 43 (14) (2010) 6075–6084.

[26] M. Alberto, et al., Study on the formation of thin film nanocomposite (TFN) membranes of polymers of intrinsic microporosity and graphene-like fillers: effect of lateral flake size and chemical functionalization, J. Membr. Sci. 565 (2018) 390–401.

[27] L. Gao, et al., High-flux PIM-1/PVDF thin film composite membranes for 1-butanol/water pervaporation, J. Membr. Sci. 529 (2017) 207–214.

[28] B.D. Cullity, Elements of X-Ray Diffraction, Addison-Wesley Publishing, 1956.

[29] H. Wu, J. Thibault, B. Kruczek, The validity of the time-lag method for the characterization of mixed-matrix membranes, J. Membr. Sci. 618 (2021), 118715.

[30] A.B. Foster, et al., Understanding the topology of the polymer of intrinsic microporosity PIM-1: cyclics, tadpoles, and network structures and their impact on membrane performance, Macromolecules 53 (2) (2020) 569–583.

[31] A. Devarajan, et al., Influence of polymer topology on gas separation membrane performance of the polymer of intrinsic microporosity PIM-py, ACS Appl. Poly. Mater. 3 (2021) 3485–3495.

[32] A.M.A. Abdelsamad, A.S.G. Khalil, M. Ulbricht, Influence of controlled functionalization of mesoporous silica nanoparticles as tailored fillers for thin-film nanocomposite membranes on desalination performance, J. Membr. Sci. 563 (2018) 149–161.

[33] S. Santos, et al., Acid-leached mixed vermiculites obtained by treatment with nitric acid, Appl. Clay Sci. 104 (2015) 286–294.

[34] L. Wang, et al., TiO_2 supported on silica nanolayers derived from vermiculite for efficient photocatalysis, Catal. Today 216 (2013) 95–103.

[35] H. Yang, et al., Preparation of Nafion/various Pt-containing SiO_2 composite membranes sulfonated via different sources of sulfonic group and their application in self-humidifying PEMFC, J. Membr. Sci. 443 (2013) 210–218.

[36] N. Majoul, S. Aouida, B. Bessaïs, Progress of porous silicon APTES-functionalization by FTIR investigations, Appl. Surf. Sci. 331 (2015) 388–391.

[37] G.H. Mirzabe, A.R. Keshtkar, Application of response surface methodology for thorium adsorption on PVA/Fe3O4/SiO2/APTES nanohybrid adsorbent, J. Ind. Eng. Chem. 26 (2015) 277–285.

[38] H. Wu, et al., Surface-modified Y zeolite-filled chitosan membrane for direct methanol fuel cell, J. Power Sources 173 (2) (2007) 842–852.

[39] H. Yang, et al., Preparation of porous material from talc by mechanochemical treatment and subsequent leaching, Appl. Clay Sci. 31 (3–4) (2006) 290–297.

[40] Z. Yan, B. Wang, K. Wang, Thermal effects on the structural response of planar serpentine interconnects, Int. J. Mech. Sci. 135 (2018) 23–30.

[41] L. Hao, K.-S. Liao, T.-S. Chung, Photo-oxidative PIM-1 based mixed matrix membranes with superior gas separation performance, J. Mater. Chem. 3 (33) (2015) 17273–17281.

[42] L. Yang, et al., Enhanced CO_2 selectivities by incorporating CO_2-philic PEG-POSS into polymers of intrinsic microporosity membrane, J. Membr. Sci. 543 (2017) 69–78.

[43] W.F. Yong, et al., Suppression of aging and plasticization in highly permeable polymers, Polymer 77 (2015) 377–386.

[44] A. Zulhairun, A. Ismail, The role of layered silicate loadings and their dispersion states on the gas separation performance of mixed matrix membrane, J. Membr. Sci. 468 (2014) 20–30.

[45] Y. Pu, et al., Amino-functionalized NUS-8 nanosheets as fillers in PIM-1 mixed matrix membranes for CO2 separations, J. Membr. Sci. 641 (2022), 119912.

[46] B. Zornoza, et al., Functionalized flexible MOFs as fillers in mixed matrix membranes for highly selective separation of CO_2 from CH_4 at elevated pressures, Chem. Commun. 47 (33) (2011) 9522–9524.

[47] B. Ghalei, et al., Enhanced selectivity in mixed matrix membranes for CO_2 capture through efficient dispersion of amine-functionalized MOF nanoparticles, Nat. Energy 2 (7) (2017) 1–9.

[48] J. Contreras-Martínez, et al., High-flux thin film composite PIM-1 membranes for butanol recovery: experimental study and process simulations, ACS Appl. Mater. Interfaces 13 (36) (2021) 42635–42649.

[49] K. Althumayri, et al., The Influence of Few-Layer Graphene on the Gas Permeability of the High-Free-Volume Polymer PIM-1, vol. 2060, Philosophical Transactions of the Royal Society a-Mathematical Physical and Engineering Sciences, 2016, p. 374.

[50] J. Ahn, et al., Polysulfone/silica nanoparticle mixed-matrix membranes for gas separation, J. Membr. Sci. 314 (1–2) (2008) 123–133.

[51] S. Mohsenpour, et al., PIM-1 membranes containing POSS - graphene oxide for CO_2 separation, Separ. Purif. Technol. 298 (2022), 121447.

[52] M. Sadeghi, M.A. Semsarzadeh, H. Moadel, Enhancement of the gas separation properties of polybenzimidazole (PBI) membrane by incorporation of silica nano particles, J. Membr. Sci. 331 (1–2) (2009) 21–30.

[53] J.H. Kim, Y.M. Lee, Gas permeation properties of poly (amide-6-b-ethylene oxide)–silica hybrid membranes, J. Membr. Sci. 193 (2) (2001) 209–225.

[54] X. Li, et al., Efficient CO_2 capture by functionalized graphene oxide nanosheets as fillers to fabricate multi-permselective mixed matrix membranes, ACS Appl. Mater. Interfaces 7 (9) (2015) 5528–5537.

[55] J. Shen, et al., Size effects of graphene oxide on mixed matrix membranes for CO_2 separation, AIChE J. 62 (8) (2016) 2843–2852.

[56] M. Mosadegh, et al., Effect of Nafion and APTEOS functionalization on mixed gas separation of PEBA-FAU membranes: experimental study and MD and GCMC simulations, Separ. Purif. Technol. 247 (2020), 116981.

[57] Q. Xin, et al., Interface engineering of mixed matrix membrane via CO_2-philic polymer brush functionalized graphene oxide nanosheets for efficient gas separation, J. Membr. Sci. 586 (2019) 23–33.

[58] J.M. Luque-Alled, et al., PIM-1/Holey Graphene Oxide Mixed Matrix Membranes for Gas Separation: Unveiling the Role of Holes, ACS applied materials & interfaces, 2021.

[59] P.M. Budd, et al., Gas permeation parameters and other physicochemical properties of a polymer of intrinsic microporosity: polybenzodioxane PIM-1, J. Membr. Sci. 325 (2) (2008) 851–860.

[60] P.M. Budd, et al., Gas separation membranes from polymers of intrinsic microporosity, J. Membr. Sci. 251 (1–2) (2005) 263–269.

[61] P. Bernardo, et al., Effect of physical aging on the gas transport and sorption in PIM-1 membranes, Polymer 113 (2017) 283–294.

[62] B. Comesaña-Gándara, et al., Redefining the Robeson upper bounds for CO 2/CH 4 and CO 2/N 2 separations using a series of ultrapermeable benzotriptycene-based polymers of intrinsic microporosity, Energy Environ. Sci. 12 (9) (2019) 2733–2740.

[63] C.R. Mason, et al., New organophilic mixed matrix membranes derived from a polymer of intrinsic microporosity and silicalite-1, Polymer 54 (9) (2013) 2222–2230.

[64] J. Ahn, et al., Gas transport behavior of mixed-matrix membranes composed of silica nanoparticles in a polymer of intrinsic microporosity (PIM-1), J. Membr. Sci. 346 (2) (2010) 280–287.

[65] Q. Song, et al., Nanofiller-tuned microporous polymer molecular sieves for energy and environmental processes, J. Mater. Chem. 4 (1) (2016) 270–279.

[66] C.H. Lau, et al., Ending aging in super glassy polymer membranes, Angew. Chem. Int. Ed. 53 (21) (2014) 5322–5326.

[67] R.S. Bhavsar, et al., Ultrahigh-permeance PIM-1 based thin film nanocomposite membranes on PAN supports for CO_2 separation, J. Membr. Sci. 564 (2018) 878–886.